JOURNAL OF COMPUTATIONAL PHYSICS 108, 1–7 (1993)

Streamline-Coordinate Finite-Difference Method for Hot Metal Deformations

S. G. CHUNG

Department of Physics, Western Michigan University, Kalamazoo, Michigan 49008

K. KUWAHARA

The Institute of Space and Astronautical Science, 3-1-1 Yoshinodai, Sagamihara, Kanagawa 229, Japan

AND

O. RICHMOND

Alcoa Laboratories, Aluminum Company of America, Alcoa Center, Pennsylvania 15069

Received December 12, 1991; revised July 30, 1992

The hot metal deformation in the rolling process is a typical example of near-steady, quasi two-dimensional non-Newtonian flows. An isotropic work-hardening model characterized by a dislocation energy-density is presented and analyzed by the streamline-coordinate finite-difference method. © 1993 Academic Press, Inc.

I. INTRODUCTION

Using a streamline coordinate in place of a Cartesian coordinate for describing laminar flows of complex matter is quite a natural idea. In particular in steady states, it is intuitively clear that the flow dynamics of complex matter accompanying free surfaces, history dependencies, and complex boundary geometry can be best analyzed by the streamline coordinate formulation. Recent studies on more or less similar ideas are due to Duda and Vrentas [1], Pearson [2], Papanastasiou *et al.* [3], and Luo and Tanner [20], yet the lack of significant efforts in further developing the idea may be due to the fact that the streamline-coordinate description is similar to the convected coordinate and full Lagrangian description [4–6] which are believed to be good only for theoretical purposes, not for practical calculations. See Refs. [7–9] for the most recent efforts. Our method is different from the previous methods in that (i) it is finite-difference and (ii) unlike the streamlined finite-element methods which solve pressure, velocity, and streamline (through stream function or other methods) simultaneously, we regard streamline as an independent coordinate and rewrite the basic equation in terms of the streamline coordinate.

This is the third in a series of papers developing the streamline-coordinate finite-difference scheme, the (x, m) scheme, for analyzing steady two-dimensional flows of non-Newtonian matter. In the previous papers [10, 11], the (x, m) scheme was examined for a modified Bingham fluid flowing through a two-dimensional converging nozzle with free-slipping boundary condition at the wall and a strain-softened Bingham-like fluid discharging from parallel plates into a free space. In the latter case, the no-slip boundary condition was imposed at the solid wall. We have so far seen no serious difficulties associated with the strong nonlinearity of the formulation, but we indeed found that the (x, m) scheme is ideal for dealing with free surfaces and history dependencies. In this paper, we will test the (x, m) scheme for a more realistic history-dependent viscoplastic matter, of which metals are good examples.

Over many years, the metal deformation processes have been analyzed almost exclusively by the finite-element methods [12–18]. The new challenges to our streamline-coordinate finite-difference scheme are: (i) the viscosity is large and varies spatially, $10^3 \sim 10^6$ (in nondimensional units), resulting from a very intricate constitutive equation and (ii) we now have two more equations to be solved for the energy density and internal dislocation density in addition to the equations of mass and momentum. The large viscosity implies a time scale L_0^2/ν, in addition to the time scale due to fluid convection L_0/U_0, where L_0 is a typical length scale and U_0 is a typical speed. Their ratio is a Reynolds number

$$(L_0^2/\nu)/(L_0/U_0) = L_0 U_0/\nu. \tag{1}$$

0021-9991/93 $5.00

As we will see later, an average Reynolds number in metal rolling processes is of order 10^{-4}, implying a very small time step in an explicit scheme, typically $\Delta t \sim 10^{-7}$. What is expected in an implicit scheme can be found by looking at the large-viscosity effect in a different way. The large viscosity means a large velocity correlation, which is similar to the situation that a large sound velocity means a large pressure correlation. In the latter, a requirement of very small time step is replaced by a large number of iterations in solving a Poisson equation in each (practical) time step. Likewise for the former, keeping the time step practical, $\Delta t \sim 10^{-3}$, one would expect a large number of iterations for an implicit evaluation of the velocity field in each time step. As for (ii) above, we will see in the text that there are no particular difficulties associated with these additional equations.

We have organized the paper as follows: In the next section, the metal deformation processes such as in the rolling will be formulated. We will examine an isotropic work-hardening model characterized by a dislocation energy density. In Section III, the basic equations described in Section II are put into the (x, m) scheme. Sections IV and V describe boundary conditions and numerical results, respectively. The summary is given in Section VI.

II. BASIC EQUATIONS

Let us consider a deformation of metals in the rolling process. We assume incompressibility, quasi-two-dimensionality, and steady states, and examine an isotropic work-hardening characterized by a dislocation energy density S. The basic equations are equations of mass, momentum, energy, internal variable S, pressure Poisson equation resulting from the first two equations, and a constitutive equation. We have [21]

$$\frac{\partial u_j}{\partial x_j} = 0 \tag{2}$$

$$\rho \frac{Du_i}{Dt} = -\frac{\partial P}{\partial x_i} + \frac{\partial}{\partial x_j}\sigma_{ij} \tag{3}$$

$$\Delta P = \frac{\partial}{\partial x_i}\frac{\partial}{\partial x_j}\sigma_{ij} - \rho \frac{\partial}{\partial x_i}\left(u_j \frac{\partial u_i}{\partial x_j}\right) - \rho \frac{\partial}{\partial t}\frac{\partial u_j}{\partial x_j} \tag{4}$$

$$\frac{DE}{Dt} = -u_j \frac{\partial P}{\partial x_j} + \frac{\partial}{\partial x_j}(u_i \sigma_{ij}) - \frac{\partial}{\partial x_j} q_j \tag{5}$$

$$\frac{DS}{Dt} = C_s \sigma_{ij} e_{ij} - \gamma e^{-\varepsilon/kT} S \tag{6}$$

$$\sigma_{ij} = 2\nu(e, S, T)\, e_{ij}. \tag{7}$$

In these equations, σ_{ij}, q_i, e_{ij}, and e, respectively, are stress tensor, heat flux, strain-rate tensor,

$$e_{ij} \equiv \frac{1}{2}\left(\frac{\partial u_i}{\partial x_j} + \frac{\partial u_j}{\partial x_i}\right), \tag{8}$$

and the magnitude of the strain-rate tensor, $e \equiv |e_{ij}| \equiv \sqrt{e_{ij} e_{ij}}$. We have defined the material derivative by

$$\frac{D}{Dt} \equiv \frac{\partial}{\partial t} + u_j \frac{\partial}{\partial x_j} \tag{9}$$

and the energy per unit volume by

$$E \equiv \frac{\rho}{2} u_i^2 + \rho C_v T + S, \tag{10}$$

where C_v is a constant volume specific heat. As for a heat conduction, we use the standard form with κ denoting a heat conductivity,

$$q_i = -\kappa \frac{\partial T}{\partial x_i}. \tag{11}$$

Equation (6) describes a work-hardening model. Note that due to Eqs. (7) and (8) $\sigma_{ij} e_{ij} = \sigma_{ij}(\partial u_i / \partial x_j)$, and thus the first term on the right of (6) is a part of the work energy

$$\frac{\partial}{\partial x_j}(u_i \sigma_{ij}) = u_i \frac{\partial}{\partial x_j}\sigma_{ij} + \sigma_{ij}\frac{\partial u_i}{\partial x_j}, \tag{12}$$

where the first term is a kinetic energy production. The energy production of the second form, the plastic work, is further divided into two parts, one used for thermal phonon creations and one for dislocation creations. The heuristic fact that about 90–95% of the second form energy is used for heat generation [14] implies that the constant

$$C_s = 0.05 \sim 0.1. \tag{13}$$

The second term on the right of (6) represents a thermal recovery with the standard Arhenius-form temperature dependence. The activation energy is known to be of order [16, 17]

$$\varepsilon = 1.5 \sim 2\ \text{eV}. \tag{14}$$

The constant γ has a dimension of s^{-1} and, from the analogy of point defect (vacancy) in solids, may be interpreted to be a jump frequency associated with the dislocation dynamics. It is reported that [16, 17]

$$\gamma = 0.38 \sim 8.55 \times 10^{12}\ \text{s}^{-1}. \tag{15}$$

The material constants (13)–(15) are for typical aluminum alloys.

Next some arguments are due on the constitutive equation (7). First of all, generally speaking, the temperature gets into the effective viscosity in two ways: one through thermal molecular vibrations and the other through the annealing process of dislocations. What was found experimentally for aluminum alloys, however, was that the temperature effect is predominantly through the annealing mechanism [12]. Thus the effective viscosity does not have an explicit temperature dependence. It was found through an experiment under the constant strain rate and isothermal conditions that temperature and strain rate appear in a unit [12]

$$\beta \equiv e/(\gamma e^{-\varepsilon/kT}). \tag{16}$$

Furthermore in history-independent cases, the experiment at elevated temperatures found an approximate viscoplastic constitutive relationship ($\sigma \equiv |\sigma_{ij}|$),

$$\sinh^n(\alpha\sigma) = \beta, \tag{17}$$

where $\alpha = 3.2 \sim 3.7 \times 10^{-8}\ \mathrm{m^2/N}$ and $n = 3.8 \sim 4.8$ [16, 17]. In our formulation, this special case (history independence) amounts to neglecting the inertial term in Eq. (6), giving

$$S = C_s \sigma \beta. \tag{18}$$

Note that $\sigma_{ij} e_{ij} = \sigma e$ are due to Eq. (7). From (7), (17), (18) we have

$$\nu(e, S) = f(s)/e \tag{19}$$

with the functional form being determined by

$$2f[C_s \sigma \cdot \sinh^n(\alpha\sigma)] = \sigma. \tag{20}$$

Considering an ambiguity in the parameters α and n, it is tempting to find an approximate elementary function for f in Eq. (20). In the rest of the paper, we will assume a simple form,

$$f(S) = \frac{1}{2\alpha} \sinh^{-1}\left(\frac{\alpha}{C_s} S\right)^{1/(n+1)}. \tag{21}$$

III. THE (x, m) SCHEME

By solving the basic equations in the last section under appropriate boundary conditions, one can find velocity profile, distributions of pressure, dislocation density, etc. If one adopts the standard Eulerian scheme, irrespective of Cartesian or natural coordinates, configuration space will be represented by discrete mesh points fixed in space. It is then immediately clear that free surfaces and history dependencies are accurately treated only with considerable difficulty. In contrast, our (x, m) scheme is ideal for dealing with free surfaces and history dependencies. It is ideal for free surfaces because the calculational space (x, m) is always rectangular no matter where the solid walls and free surfaces. We do not need to know actual locations of free surfaces during the evaluation of velocity field, pressure field, etc. It is also ideal for history dependencies because, as we will see below, one can evaluate the internal variable at each time step quite easily and accurately.

Before we introduce the (x, m) scheme, we make the basic equations nondimensional, which is convenient for our discussions and numerical calculations below. Let us scale length by a representative length L_0, speed by a representative speed U_0 and therefore time by L_0/U_0. In the rolling process, L_0 is taken to be the inlet width and U_0 to be the roller speed. Quantities P, σ_{ij}, E, and S all have the same dimensions and are scaled by ρU_0^2. As for the heat flux and temperature, they are scaled by ρU_0^3 and the inlet temperature T_0, respectively. Nondimensionalized equations for velocity, pressure, dislocation density, temperature, and effective viscosity read

$$\frac{Du_i}{Dt} = -\frac{\partial P}{\partial x_i} + \frac{\partial}{\partial x_j}\sigma_{ij} \tag{22}$$

$$\Delta P = \frac{\partial}{\partial x_i}\frac{\partial}{\partial x_j}\sigma_{ij} - \frac{\partial}{\partial x_i}\left(u_j \frac{\partial u_i}{\partial x_j}\right) - \frac{\partial}{\partial t}\frac{\partial u_j}{\partial x_j} \tag{23}$$

$$\frac{DS}{Dt} = C_s \sigma e - C_2 e^{-C_5/T} \cdot S \tag{24}$$

$$\frac{DT}{Dt} = \frac{1}{C_1}\{(1 - C_s)\sigma e + C_2 e^{-C_5/T} S\} + C_4 \Delta T \tag{25}$$

$$\nu(e, S) = \frac{1}{2C_3 e} \sinh^{-1}(C_3 S/C_s)^{1/n+1}. \tag{26}$$

In these equations, Eq. (25) is derived from Eqs. (5), (10), and (11), and (26) from Eqs. (19) and (21). Nondimensional parameters are defined in Table I.

We are now ready to introduce a streamline coordinate m

TABLE I

Nondimensional Parameters

$C_1 = C_v T_0/U_0^2$
$C_2 = \gamma L_0/U_0$
$C_3 = \alpha\rho U_0^2$
$C_4 = \kappa/(\rho C_v L_0 U_0)$
$C_5 = \varepsilon/kT_0$
$C_6 = hL_0/\kappa$

and regard the Cartesian y component as a dependent variable:

$$y = y(x, m). \tag{27}$$

The incompressibility Eq. (2) reduces to

$$uy_m = \text{independent of } x \equiv U(m). \tag{28}$$

From now on we use the notion (u, v) for the x and y components of velocity and subscript x or m means a partial differentiation. With Eq. (28) and the definition

$$y_x = v/u, \tag{29}$$

the differential operators transform as

$$\partial_x \to \partial_x - (v/U)\,\partial_m \tag{30a}$$

$$\partial_y \to (u/U)\,\partial_m. \tag{30b}$$

An important aspect of transformation (30) is that it does not explicitly contain the unknown $y(x, m)$. This implies that the (x, m) scheme has a particular benefit for dealing with free surfaces, since we do not need to know the streamline positions including free surfaces during the course of evaluation of other variables. The streamline positions can be easily found by solving the Poisson equation

$$(\partial_{xx} + \partial_{mm})\, y = (v/u)_x + (U/u)_m \tag{31}$$

after the velocity field is obtained.

The (x, m) scheme is also ideal for analyzing history-dependent cases. To see this we apply the transformation (30) to Eq. (24). The resulting equation

$$u\frac{\partial S}{\partial x} = C_s \sigma e - C_2 e^{-C_5/T} S \tag{32}$$

can be analytically integrated to give

$$S(x, m) = S(x_0, m) + C_s e^{-g(x,m)} \times \int_{x_0}^{x} \left[\frac{\sigma e}{u}\exp(g)\right](x', m)\, dx', \tag{33}$$

where x_0 denotes the inlet position and

$$g(x, m) \equiv \int_{x_0}^{x} \frac{(C_2 e^{-C_5/T})}{u}(x', m)\, dx'. \tag{34}$$

A question which we have deliberately avoided up to this point is if our work-hardening model is consistent with the constant strain rate, isothermal experiment reporting that temperature and strain rate appear as the unit, Eq. (16). The answer to this question is affirmative as follows: Consider a unidirectional tensile situation. One then has

$$u = ex \quad \text{and} \quad v = -ey \tag{35}$$

and Eq. (32) reduces to

$$x\frac{dS}{dx} = \sqrt{2}\, C_s \sigma - (C_2 e^{-C_5/T}/e) S. \tag{36}$$

Since σ is a function of only S, as is seen in Eq. (26) or, more precisely, Eq. (19), Eq. (36) implies that S and, therefore, σ too depend on temperature and strain rate only through the unit Eq. (16), which is what we are looking for.

IV. BOUNDARY CONDITIONS

We solve the coupled equations for velocity, pressure, dislocation density, and temperature in the (x, m) scheme by a finite difference approximation. As an illustration of the finite difference approximation, we give an explicit form for the case of temperature. Equation (25) is first expressed in terms of the (x, m) coordinates through the transformation (27) and (30), and then it is approximated as

$$\frac{T(i,j) - T0(i,j)}{\Delta t} + u(i,j)\frac{T(i+1,j) - T(i-1,j)}{2\Delta x} = \frac{1}{C_1}\{(1 - C_s)\,\sigma e - C_2 e^{-C_5/T0} S\}(i,j) + C_4\,\Delta T \tag{37}$$

with

$$\begin{aligned}\Delta T = {} & \{T(i+1,j) - 2T(i,j) + T(i-1,j)\}/\Delta x^2 \\ & - CY(i,j) \times \{T(i+1,j+1) - T(i+1,j-1) \\ & - T(i-1,j+1) + T(i-1,j-1)\}/(2\Delta x\,\Delta m) \\ & + (CX^2 + CY^2)(i,j) \times \{T(i,j+1) - 2T(i,j) \\ & + T(i,j-1)\}/\Delta m^2 + [-\{CY(i+1,j) \\ & - CY(i-1,j)\}/2\Delta x \\ & + CY(i,j) \times \{CY(i,j+1) - CY(i,j-1)\}/2\Delta m \\ & + CX(i,j) \cdot \{CX(i,j+1) - CX(i,j-1)\}/2\Delta m] \\ & \times \{T(i,j+1) - T(i,j-1)\}/2\Delta m,\end{aligned} \tag{38}$$

where we have abbreviated as $CX \equiv u/U$ and $CY \equiv v/U$. Equation (37) is solved iteratively for temperature using the old temperature $T0(i, j)$ and other quantities.

The final ingredient in numerical calculations is a bunch of boundary conditions, which we will now discuss for each

quantity: (i) *Velocity*. There are two types of boundaries, slab-roller interfaces and free surfaces. At the slab-roller interfaces, we assume no-relative-slip situation. Depending on the condition at interfaces, a partial-slip situation or more intricate boundary conditions may be appropriate [17, 18]. As for free surfaces, the boundary condition for the velocity field is that the stress tensor is zero. Note that both the pressure and the stress tensor are generally discontinuous across the free surfaces [3, 11]. In finite-difference methods, it is technically convenient to deal with the vacuum-side values. After transforming to the (x, m) coordinates, we have [11]

$$u_m = vu_x U/(u^2+v^2) \tag{39a}$$

$$v_m = vv_x U/(u^2+v^2). \tag{39b}$$

An important note here is that one of the two separation points at the front and rear sides of the rollers should be found as a part of the solution. We fix the front separation point and solve for velocity and slab thickness at the inlet, whereas we let the rear separation point vary move until the streamlines become as smooth as possible near the rear separation point, which will be realized as the most stable state (see an argument given in the last paper in Ref. [20], although we believe that their argument needs further clarification). (ii) *Pressure*. At the free surfaces, in consistency with the velocity boundary condition above, the pressure is put equal to zero, the ambient, vacuum side value. As in the standard Eulerian scheme for solving the Navier–Stokes equation, pressure at all the other boundaries are evaluated using Eq. (22). (iii) *Temperature*. Finally, for the temperature, we fix the entering temperature $T = T_0$ and impose a convective cooling at the surfaces

$$q_j n_j = h(T - T_\infty), \tag{40}$$

where n_j is the unit vector normal to the surface, h is a convection coefficient, and T_∞ is the ambient temperature. One can use different h's for free surfaces and roller-material interfaces, but here we use a single h for simplicity. The nondimensional form of Eq. (40) in the (x, m) space gives

$$T_m = \{C_6\sqrt{u^2+v^2}\,(T - T_\infty/T_0) + vT_x\}/(CX\cdot u + CY\cdot v). \tag{41}$$

V. NUMERICAL RESULTS

All the physical parameters of aluminum alloys as used in our numerical calculations are listed in Table II. The geometry of the metal rolling process we have analyzed will be clear from the figures. Table III summarizes geometrical information, mesh sizes, etc.

As in our second paper [11], we use MAC method for the pressure Poisson equation and the implicit method for velocity and temperature. The Poisson equation for the streamline (31) can be solved by the same procedure as for pressure using $y_x = v/u$ and $y_m = U/u$ as boundary conditions. We have solved the full coupled equations (22), (23), (25), (26), and (33) for velocity, pressure, effective viscosity, dislocation density, and temperature in four steps: In step 1, we solve the Newtonian case with constant viscosity $v = 10^3$. In step 2, using the solution of step 1 as initial input, we solve the viscoplastic case with the constitutive equation (17). In step 3, using the solution of step 2 as initial input, we solve the history-dependent viscoplastic case. The temperature is held constant so far. In the final step 4, using the solution of step 3 as initial input, we solve the history-dependent viscoplastic case with temperature effect. Since the temperature effect was found to be small in our situation, the result of step 3 will not be presented here. To obtain the numerical results below, iterations were continued until the convergence criterion was satisfied,

$$\sum_{i,j} |u^m(i,j) - u^{m+1}(i,j)| \Big/ \sum_{i,j} |u^m(i,j)| < 10^{-6}, \tag{42}$$

where m represents the mth step of iteration.

In Fig. 1, we compare velocity profiles for the three cases. Except for some differences at the entrance and about 10% reduction in the outlet slab width in the latter two cases, compared with the Newtonian case (top), velocity profiles

TABLE II

Aluminum Properties Used in Calculations

Density	$\rho = 2700$ kg/m^3
Specific heat	$C_v = 963$ J/kg · K
Thermal conductivity	$\kappa = 200$ W/mK
Convection coefficient	$h = 20$ W/m^{2}K
Activation energy of dislocations	$\varepsilon = 17400$ K
Parameters for viscoplastic flow	$n = 4$
	$C_s = 0.1$
	$\gamma = 10^{12}$/s
	$\alpha = 3 \times 10^{-8}$ m^2/N

TABLE III

Size, Mesh, etc., Used in Calculations

Inlet width	$L_0 = 0.04$ m
Throat width	$= 0.016$ m
Roller speed	$U_0 = 1.0$ m/s
Roller radius	$= 0.0727$ m
Inlet temperature	$T_0 = 600$ K
Ambient temperature	$T_\infty = 300$ K
Mesh size	$\Delta x = 0.05$
	$\Delta m = 0.05$
	$\Delta t = 0.001$

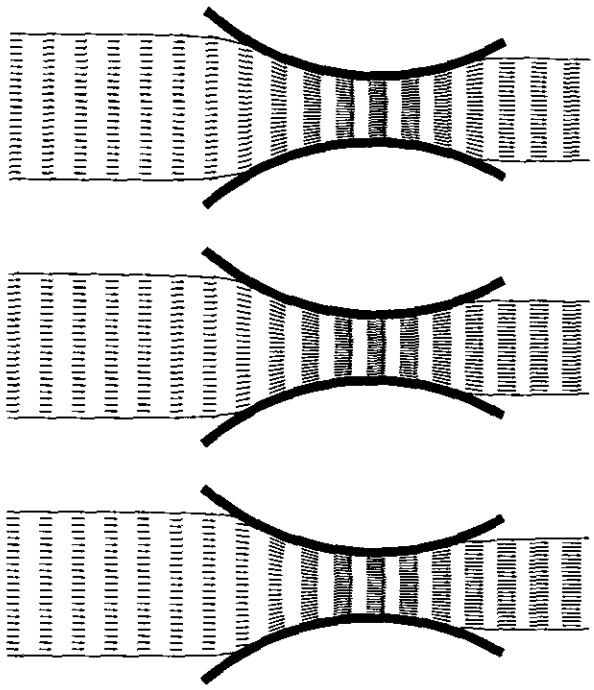

FIG. 1. Velocity profiles for, from top to bottom, the Newtonian case with $\nu = 10^3$, the viscoplastic case, and the history-dependent viscoplastic case.

are rather similar to each other, clearly due to large viscosities.

Figure 2 compares pressure profiles. In the Newtonian case, a large maximum (left) and a minimum (right) are observed near the front separation point, and a small

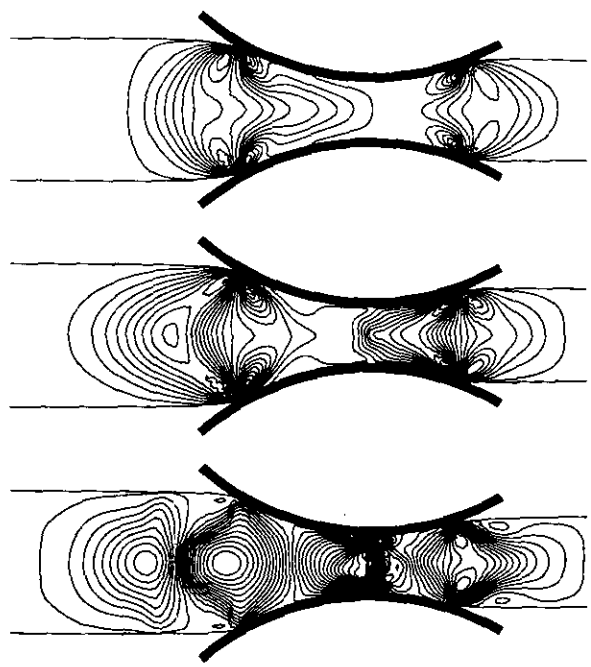

FIG. 2. Pressure contours corresponding to the velocity profiles in Fig. 1.

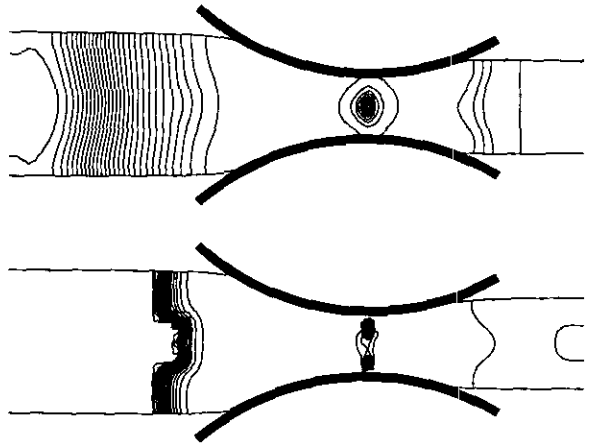

FIG. 3. Viscosity contours for the viscoplastic case (top) and the history-dependent viscoplastic case (bottom).

maximum (left) and a minimum (right) are observed near the rear separation point. Here $P_{\min} = -32$ atm. and $P_{\max} = 37$ atm. Moving to the viscoplastic case, the only change from the Newtonian case is that the front maximum is weakened and the rear one strengthened. Here $P_{\min} = -33$ atm. and $P_{\max} = 41$ atm. Moving further to the history-dependent case, the min–max pair structures near the separation points are replaced by new structures centered on the symmetry axis. Downstream we see a weak maximum followed by a large minimum, then a strong maximum near the throat area, and finally a maximum near the exit. Here $P_{\min} = -149$ atm. and $P_{\max} = 182$ atm.

Figure 3 compares the effective viscosity in the viscoplastic case with that in the history-dependent case. $\nu_{\min} = 1.2 \times 10^5$, $\nu_{\max} = 6.0 \times 10^6$ in the viscoplastic case, and $\nu_{\min} = 6.6 \times 10^4$, $\nu_{\max} = 5.5 \times 10^8$ N · s/m^2 in the history-dependent case. Since the effective viscosity is, roughly speaking, inversely proportional to strain rate, a maximum structure near the throat area indicates a relatively uniform

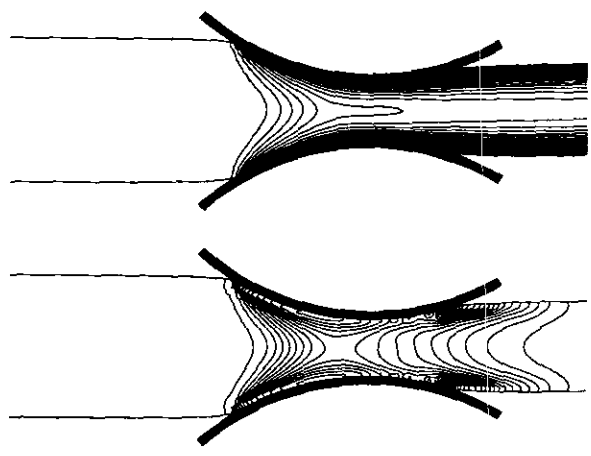

FIG. 4. Contours of dislocation density (top) and temperature (bottom) in the history-dependent viscoplastic case.

motion in agreement with intuition. The work-hardening effect simply enhances rigid motion, leading to larger effective viscosity. Figure 4 represents the profiles of dislocation density and temperature distributions in the history-dependent viscoplastic case. As is expected, the dislocation density monotonously increases from inlet to outlet along the streamline, with the largest dislocation being realized at the free surfaces. $S_{\min} = 7.6 \times 10^4$ and $S_{\max} = 8.72 \times 10^6$ J/m^3. If one roughly estimates the average dislocation energy to be 50 eV, then our result amounts to $10^{10} \sim 10^{12}$ dislocations/cm^2 which is a typical value for heavily deformed metals [19]. As for temperature, it first increases due to deformation, getting highest near the rear separation point and then cools down toward the outlet due to conduction and convection, $T_{\min} = 594$ K and $T_{\max} = 624$ K.

VI. SUMMARY

In this paper, we have analyzed the metal rolling process as a typical example of history-dependent viscoplastic flows, using the streamline-coordinate finite-difference method. We have demonstrated that the (x, m) scheme is ideal for dealing with steady non-Newtonian flows with free surfaces and history dependencies. As to the question of how troublesome the strong nonlinearity of the streamline coordinate formulation, simply because of lack of nonlinear stability theory, the only way to answer the question is to solve a variety of complex flows. Although our numerical results for the isotropic work-hardening model look physically reasonable, the most realistic models such as a tentorial, or directional, hardening model or including viscoelasticity are yet to be explored before we start comparing numerical results with various experiments. The analysis of steady non-Newtonian flows with a tentorial-hardening property and/or viscoelasticity is certainly a tough challenge to the streamline-coordinate finite-difference method.

ACKNOWLEDGMENTS

This work was supported by ALCOA, Aluminum Company of America and ICFD, Institute of Computational Fluid Dynamics. SGC thanks members of ICFD for their help and hospitality. Special thanks are due to M. Suito for generating some numerical results.

REFERENCES

1. J. L. Duda and J. S. Vrentas, *Chem. Eng. Sci.* **22**, 855 (1967).
2. C. E. Pearson, *J. Comput. Phys.* **42**, 257 (1981).
3. A. C. Papanastasiou, C. W. Macosko, and L. E. Scriven, in *Finite Elements in Fluids*, edited by R. H. Gallagher *et al.* (Wiley, London, 1985), Vol. 6, p. 263; A. C. Pananastasiou, L. E. Scriven, and C. W. Macosko, *J. Non-Newtonian Fluid Mech.* **22**, 271 (1987).
4. J. G. Oldroyd, *Proc. R. Soc. London Ser. A* **200**, 523 (1950); **245**, 278 (1958).
5. Iu. Z. Povstenko and Ia. S. Podstrigach, *Fz. Met. Metalloved.* **47**, 832 (1983) [*Phys. Met. Metallogr. (USSR)* **47**, 827 (1983)].
6. C. J. M. Gelten and A. W. A. Konter, in *Numerical Methods in Industrial Forming Processes* (Swansea, UK, 1982), pp. 511–521.
7. S. Ghosh, *J. Mater. Shaping Technol.* **8**, 53 (1990).
8. S. Ghosh and N. Kikuchi, preprint.
9. S. F. Hoysan and P. S. Steif, preprint.
10. S. G. Chung, S. C.-Y. Lu and O. Richmond, *Phys. Rev. A* **39**, 2728 (1989).
11. S. G. Chung and K. Kuwahara, *J. Comput. Phys.*, in press.
12. U. S. Lindholm, *Appl. Mech. Rev.* **43**, 338 (1990).
13. A. D. Freed and K. P. Walker, *Appl. Mech. Rev.* **43**, 328 (1990).
14. D. J. Bammann, *Appl. Mech. Rev.* **43**, 312 (1990).
15. O. Richmond, *J. Metals* **16** (1986).
16. R. E. Smelser and O. Richmond, in *Proceedings, NUMIFOM'86 Conference*, p. 305.
17. P. R. Dawson, *Int. J. Mech. Sci.* **26**, 227 (1984).
18. O. C. Zienkiewicz, P. C. Jain, and E. Onate, *Int. J. Solids Struct.* **14**, 15 (1978).
19. C. Kittel, *Introduction to Solid State Physics* (6th ed.) (Wiley, New York, 1986), Chap. 20.
20. X. Luo and R. I. Tanner, *J. Non-Newtonian Fluid Mech.* **21**, 61 (1986); **22**, 61 (1986); **31**, 143 (1989). Their recent paper, **28**, 149 (1988), analyzes a rolling (calendering) deformation of viscoelastic fluids.
21. See, for the time-dependent term in the pressure Poisson equation (4), F. H. Harlow and J. E. Welch, *Phys. Fluids* **8**, 2182 (1965).